Protein Engineering, Design & Selection vol. 23 no. 4 pp. 243–249, 2010
Published online January 6, 2010 doi:10.1093/protein/gzp081

ImmunoPET imaging of B-cell lymphoma using ^{124}I-anti-CD20 scFv dimers (diabodies)

Tove Olafsen[1,4], Shannon J.Sirk[1], David J.Betting[2], Vania E.Kenanova[1], Karl B.Bauer[1], Waldemar Ladno[1], Andrew A.Raubitschek[3], John M.Timmerman[2] and Anna M.Wu[1]

[1]Department of Molecular and Medical Pharmacology, UCLA Crump Institute for Molecular Imaging, California NanoSystems Institute, Room 4350B, 570 Westwood Plaza, Building 114, Box 951770, Los Angeles, CA 90095, USA, [2]UCLA Department of Medical Hematology and Oncology, David Geffen School of Medicine at University of California, Center for the Health Sciences, 10833 Le Conte Avenue, Los Angeles, CA 90095, USA and [3]Department of Radioimmunotherapy, City of Hope National Medical Center, 1500 East Duarte Road, Duarte, CA 91010, USA

[4]To whom correspondence should be addressed.
E-mail: tolafsen@mednet.ucla.edu

Received November 30, 2009; revised November 30, 2009; accepted December 1, 2009

Edited by Paul Carter

Rapid clearing engineered antibody fragments for immunoPET promise high sensitivity at early time points. Here, tumor targeting of anti-CD20 diabodies (scFv dimers) for detection of low-grade B-cell lymphomas were evaluated. In addition, the effect of linker length on oligomerization of the diabody was investigated. Four rituximab scFv variants in the V_L-V_H orientation with different linker lengths between the V domains (scFv-1, scFv-3, scFv-5, scFv-8), plus the scFv-5 with a C-terminal cysteine (Cys-Db) for site-specific modification were generated. The scFv-8 and Cys-Db were radioiodinated with ^{124}I for PET imaging, and biodistribution of ^{131}I-Cys-Db was carried out at 2, 4 10 and 20 h. The five anti-CD20 scFv variants were expressed as fully functional dimers. Shortening the linker to three or one residue did not produce higher order of multimers. Both ^{124}I-labeled scFv-8 and Cys-Db exhibited similar tumor targeting at 8 h post injection, with significantly higher uptakes than in control tumors ($P < 0.05$). At 20 h, less than 1% ID/g of ^{131}I-labeled Cys-Db was present in tumors and tissues. Specific tumor targeting and high contrast images were achieved with the anti-CD20 diabodies. These agents extend the repertoire of reagents that can potentially be used to improve detection of low-grade lymphomas.

Keywords: CD20/lymphoma model/PET/scFv

Introduction

Radiolabeled antibodies offer the possibility to target tumor surface antigens for immunotherapy and immunoimaging. However, intact antibodies are large proteins with long serum half-lives and low penetration into tumors. The prolonged residence time in the blood and subsequently extensive radioactive exposure to normal organs can be toxic and lead to organ failure. To overcome the limitations of intact antibodies, protein engineering has been employed to produce smaller antibody fragments such as single-chain Fv (scFv; ~25 kDa) and diabodies (scFv dimers; ~50 kDa) (Bird *et al*., 1988; Huston *et al*., 1988; Holliger *et al*., 1993). Due to their smaller size, these fragments exhibit improved tumor penetration and rapid clearance from the blood through the kidneys. Studies comparing the two fragments have shown that the larger-sized diabody with two antigen binding sites has better tumor retention than the smaller monovalent scFv (Adams *et al*., 1993; Wu *et al*., 1996; Adams *et al*., 1998). More recently, expression of the carcinoembryonic antigen (CEA; colon cancer) and the Her2/neu growth factor receptor (breast cancer) were visualized by positron emission tomography (PET) using ^{124}I-labeled T84.66 and ^{124}I-labeled C6.5 diabodies as immunoPET tracers, respectively (Sundaresan *et al*., 2003; Robinson *et al*., 2005). Although larger antibody fragments such as dimers of scFv-C_H3 (minibodies; ~80 kDa) and scFv-Fc (~105 kDa) also show excellent properties with regards to tumor uptake due to their longer blood clearance (Wu and Senter, 2005), diabodies offer the possibility for same-day imaging. Furthermore, the biological half-life of the diabody (3–5 h) is compatible with the physical half-life of ^{18}F (109 min) which could be advantageous with regard to clinical translation.

It has been shown that a linker length of 12 residues or less between the variable (V) domains will force the scFv to cross-link with another scFv to form a dimer (diabody) (Kortt *et al*., 1994; Whitlow *et al*., 1994). Investigation into the effect of shorter linkers (three residues and less) has shown that higher orders of scFv multimerization such as trimers and tetramers occurs (Dolezal *et al*., 2000). Increasing the valency of a scFv fragment offers the prospect of improved tumor uptake due to improved functional affinity (avidity), while retaining rapid blood clearance. Indeed, excellent *in vivo* targeting was demonstrated in a recent study of a 0-linker anti-Lewis Y scFv that multimerized into trimer/tetramer species (Kelly *et al*., 2008). However, the transition into multimers is not absolute and appears to be dependent on several factors such as the antibody sequence, the orientation of the V domains, the intrinsic stabilities of the domains and the dissociation equilibrium of the V_L-V_H interface (Arndt *et al*., 1998; Worn and Pluckthun, 1999).

ImmunoPET imaging requires that the antibody fragment must be radiolabeled with a positron emitting radionuclide prior to administration. Common radiolabeling chemistries involve random modification of lysine or tyrosine residues. As the antibody fragment gets smaller, there is a higher probability that alteration of random tyrosines and lysines will disrupt the antigen binding site and/or the overall conformation of the molecule, leading to reduction or loss of biological function (immunoreactivity) after radiolabeling. Furthermore, the radiolabeling occurs with unknown stoichiometry, resulting in potential variability in the final radiolabeled product. One strategy to overcome these issues

is to introduce a C-terminal cysteine residue that can allow site-specific, thiol-mediated conjugation chemistry at a location physically separated from the antigen-binding sites (Li *et al*., 2002). We have previously described an anti-CEA cysteine-diabody (Cys-Db) and shown that it exists as stable covalent dimer which can be reduced to expose free thiols and modified (Olafsen *et al*., 2004a). The cysteines were radiometal labeled with the positron emitter ^{64}Cu ($t_{1/2} = 12.7$ h) and the fragment was evaluated by PET imaging in tumor-bearing mice. Specific tumor uptake was observed at 4 and 18 h post injection (p.i.). Hence, the location and number of cysteines (1 per scFv subunit, 2 per diabody) bypasses the issues associated with randomly located, stoichiometrically variable conjugation techniques. The Cys-Db format was recently extended to two additional targets, CD20 (B-cell lymphomas) and Her2/neu (Sirk *et al*., 2008). *In vitro* characterization of these fragments showed that the C-terminal cysteines could be readily modified, demonstrating the versatility and reproducibility of the system.

The objective of this work was to evaluate *in vivo* tumor targeting and PET imaging of an ^{124}I-labeled anti-CD20 diabody. In addition, the effect of the linker length between the variable domains was evaluated. A total of five different scFv variants were generated from the variable domains of the chimeric (mouse/human) anti-CD20 antibody rituximab C2B8 (Rituxan®, Genentech/Biogen-IDEC, San Francisco, CA, USA). The variants were assessed for binding to CD20 and size was determined by size-exclusion chromatography. The anti-CD20 scFv dimer with eight residues linker (scFv-8) and Cys-Db (Sirk *et al*., 2008) was randomly radioiodinated with ^{124}I and evaluated for their ability to image CD20 positive tumors. In addition, the Cys-Db was radioiodinated with ^{131}I for biodistribution studies.

Material and methods

Construction, expression and selection

The isolation of the anti-CD20 2B8 variable (V) genes has been described (Olafsen *et al*., 2009). In order to produce scFv fragments with different linker lengths (eight, five, three and one residues), individual V-genes were amplified by PCR using the scFv-Fc as template (Olafsen *et al*., 2009), followed by splice overlap extension PCR (SOE-PCR). All constructs were made in the V_L–V_H orientation. The resulting four constructs were cloned into pCR2.1-TOPO vector (Invitrogen Corporation, Carlsbad, CA, USA) and verified by sequencing. The scFv construct with 5-residue linker (scFv-5) was subjected to *in vitro* mutagenesis to append the GGC sequence (Sirk *et al*., 2008).

All five scFv constructs were subcloned into the mammalian pEE12 expression vector on *XbaI-EcoRI* sites, and expressed in NS0 myeloma cells following transfection and selection in glutamine deficient media as described (Olafsen *et al*., 2006). Clones expressing scFv fragments were identified by western blots, using alkaline phosphatase (AP) conjugated goat anti-mouse Fab-specific antibody for detection (Jackson ImmunoResearch Laboratories, West Grove, PA, USA), and expanded to triple flasks.

Purification

Protein (scFv) from terminally grown cultures was purified either by ion-exchange chromatography or by affinity chromatography. For ion-exchange chromatography, a two-step purification scheme with anion exchange followed by cation exchange was employed. Supernatants from clones expressing scFv fragments were treated with 5% AG1-X8, 100–200 mesh (BioRad Laboratories, Hercules, CA, USA); buffer exchanged to 50 mM HEPES (pH 7.0) before being loaded onto an anion exchange column (Source 15Q, GE Healthcare Life Sciences, Piscataway, NJ, USA). Bound protein was eluted with a gradient from 0–40 mM NaCl in the presence of 50 mM HEPES (pH 7.0). When eluted fractions were examined for presence of protein, it was found that the scFv was in the flow through. The flow through was concentrated using Labscale™ TFF system (Millipore, Billerica, MA, USA), buffer exchanged to 50 mM acetic acid (pH 5.0) and loaded onto a cation exchange column. Bound proteins were eluted with a gradient from 0 to 62.5 mM NaCl in the presence of 50 mM acetic acid (pH 5.0). The Cys-Db was also purified by protein L affinity chromatography. Supernatant was passed over a protein L agarose column (Thermo Fisher Scientific Inc., Rockford, IL, USA) and eluted with 0.2 M citrate buffer (pH 2.1) as described (Olafsen *et al*., 2009). Eluted fractions from ion-exchange or affinity chromatography were dialyzed against PBS at 4°C, concentrated down to about 0.5 ml as described (Olafsen *et al*., 2009). Readings at A_{280} were used to determine the concentration of the proteins, using the extinction coefficient ϵ 1.4 mg/ml.

In vitro characterization

Aliquots of purified protein were loaded onto pre-cast SDS–PAGE gels (4–20%; BioRad Laboratories) under non-reducing conditions. The Cys-Db was also analyzed under reducing conditions using 1 mm DTT. The gel was stained with MicrowaveBlue (Protiga, Frederick, MD, USA) to visualize the bands. Purified proteins (~50 μg) were subjected to size exclusion chromatography on Superdex 75 HR 10/30 (GE Healthcare Life Sciences) using a 0.5 ml flow rate and PBS. Retention time was compared with that of the anti-CEA Cys-Db (Olafsen *et al*., 2004a) and to molecular weight markers that ranged from 12.4 to 200 kDa in size (Sigma, Saint Louis, MO, USA). Binding was assessed by indirect immunofluorescence using murine B-cell lymphoma 38C13 transduced with human huCD20 (Olafsen *et al*., 2009). Cells (5×10^5) were incubated for 1 h on ice with 500 μl diabody at 5 μg/ml concentration in PBS/1% fetal bovine serum (FBS). Cells were washed and stained with phycoerythrin (PE) conjugated goat anti-mouse (Fab specific) antibodies (Jackson ImmunoResearch) at 1:100 dilution for detection.

Radioidination

For PET imaging, purified rituximab scFv-8 and Cys-Db (0.1 mg) were radioiodinated with 0.422 and 0.633 mCi, respectively, with the positron emitting isotope ^{124}I (sodium iodide in 0.02 M NaOH) provided by IBA Molecular (Sterling, VA, USA) as previously described (Kenanova *et al*., 2005; Olafsen *et al*., 2006). Instant thin-layer chromatography using the Monoclonal Antibody ITLC Strips Kit (Biodex Medical Systems, Shirley, NY, USA) was used to

determine the labeling efficiency as described (Olafsen *et al*., 2006). Immunoreactivity was assayed by incubating radioiodinated protein with an excess amount of 38C13-huCD20 cells for 1 h, centrifuging the cells and counting activity remaining in the supernatant. The labeling efficiencies ranged from 78.9 to 85.6%, and the immunoreactivity was 29.2 and 40.0% for scFv-8 and Cys-Db, respectively. Additionally, for biodistribution studies, 150 μg of Cys-Db was radioiodinated with 223 μCi of ^{131}I (PerkinElmer Life and Analytical Sciences Inc., Boston, MA, USA). The labeling efficiency for this reaction was 73.5%.

Animal studies

Six- to 8-week-old female C3Hf/Sed/Kam mice were bred and housed at the UCLA Defined Pathogen Colony according to an approved UCLA's Chancellor's Animal Research Committee protocol. The 38C13 (Bergman and Haimovich, 1977) and 38C13-huCD20 cells were propagated in RPMI supplemented with 10% FBS, 1% Penicillin (10 000 units/ml), 1% Streptomycin (10 000 μg/ml), 1% Glutamine (29.2 mg/ml) and 50 μM 2-mercaptoethanol (all from Invitrogen Corp.). Tumors were established by subcutaneous injection of 5×10^3 cells in each shoulder region as described (Olafsen *et al*., 2004b; Kenanova *et al*., 2005). Following i.v. injection of radioactivity, mice were either imaged or sacrificed for biodistribution studies.

For PET imaging, groups of four mice were injected with ^{124}I-labeled diabody. After 8 h, mice were anesthetized with 2% isoflurane and imaged for 10 min (one bed position) in a Focus 220 microPET scanner (Siemens Preclinical Solutions, Knoxville, TN, USA) followed by a 10 min scan in the microCATII (Concorde Microsystems, Knoxville, TN, USA) instrument. The mice were then euthanized, and tumors and organs were excised, weighed and counted in a Wallac WIZARD Automatic Gamma Counter (PerkinElmer Life and Analytical Sciences Inc.). After decay correction, the percent injected dose per gram (ID/g) was calculated, correcting for the labeling efficiency and immunoreactivity of each protein. The microPET and microCT scans were co-registered to yield a single image that were displayed using AMIDE (Loening and Gambhir, 2003) and regions of interest (ROIs) were drawn as described (Sundaresan *et al*., 2003) to calculate positive tumor to negative tumor and soft tissue ratios.

For biodistribution studies, mice were injected with ^{131}I-labeled diabody. At selected time points (2, 4, 10 and 20 h), groups of four mice were sacrificed, tumors and organs were harvested and percent ID/g was determined as described (Yazaki *et al*., 2001). All significance testing was done at 0.05 confidence level using Student's *t*-test.

Results

In vitro characterization of anti-CD20 diabodies

SDS–PAGE A total of five different anti-CD20 scFv variants were generated in the V_L–V_H orientation. Four scFv fragments differed in the linker length (eight, five, three and one residues) between the variable domains (Fig. 1). In addition one variant, scFv-5, was appended with a C-terminal cysteine preceded by two glycines to make a Cys-Db for the purpose of enabling site-specific modification. The five scFv variants were expressed and purified from terminal mammalian cell cultures. The size and purity of the scFv variants following purification was evaluated by SDS–PAGE (Fig. 2A). The non-covalently bound scFv fragments migrated as a monomer consistent with their predicted molecular weight of ~25 kDa (lanes 1–4), and the covalent bound Cys-Db as ~50 kDa (lane 5) under non-reducing conditions. When the Cys-Db was reduced, it migrated as a monomer (lane 6) confirming that disulfide bonds were broken between the scFv dimers in this molecule.

Size exclusion Size-exclusion chromatography was carried out in order to evaluate the native conformation of the scFv variants in solution. All the scFv variants eluted earlier (~23 min) than the carbonic anhydrase of 29 kDa (24.7 min) and later than the alcohol dehydrogenase of 150 kDa (21.8 min) as expected for a scFv dimer with an approximately molecular weight of 50 kDa (Fig. 2B). The Cys-Db eluted at a time slightly later than the non-covalently bound scFv variants with 8-, 5- and 3-residue linker, suggesting that it is a smaller, probably more compact molecule. This is not unexpected as a similar difference in size was previously observed with the anti-CEA Cys-Db (Olafsen *et al*., 2004a). However, reducing the linker length to 3 or 1 amino acids did not promote higher order multimers of this fragment.

Flow cytometry In order to evaluate function of the scFv variants, binding to CD20 was demonstrated by indirect immunofluorescence staining of 38C13-huCD20 cells incubated with purified protein. As can be seen in Fig. 2C, all of the scFv variants shifted the mean fluorescence intensity of the cells to the right, indicating specific binding.

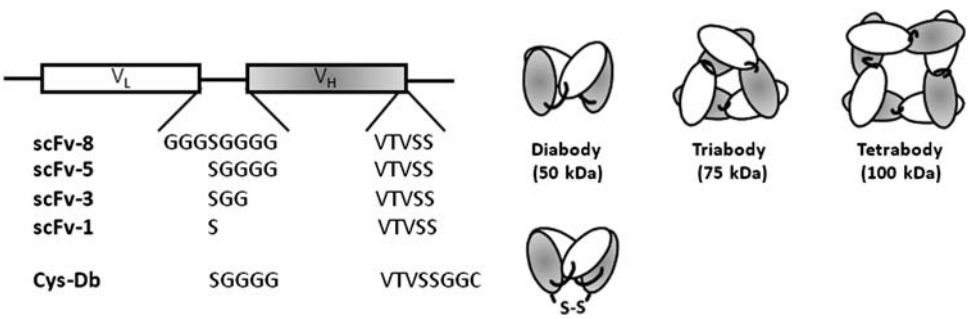

Fig. 1. Schematic presentation of the genes encoding the anti-CD20 scFv with the different linker lengths shown. V_L = variable light; V_H = variable heavy. The dimer (diabody), trimer (triabody) and tetramer (tetrabody) are shown with their molecular masses below in parentheses. The Cys-Db with its appended cysteine residue at the C-termini is also shown.

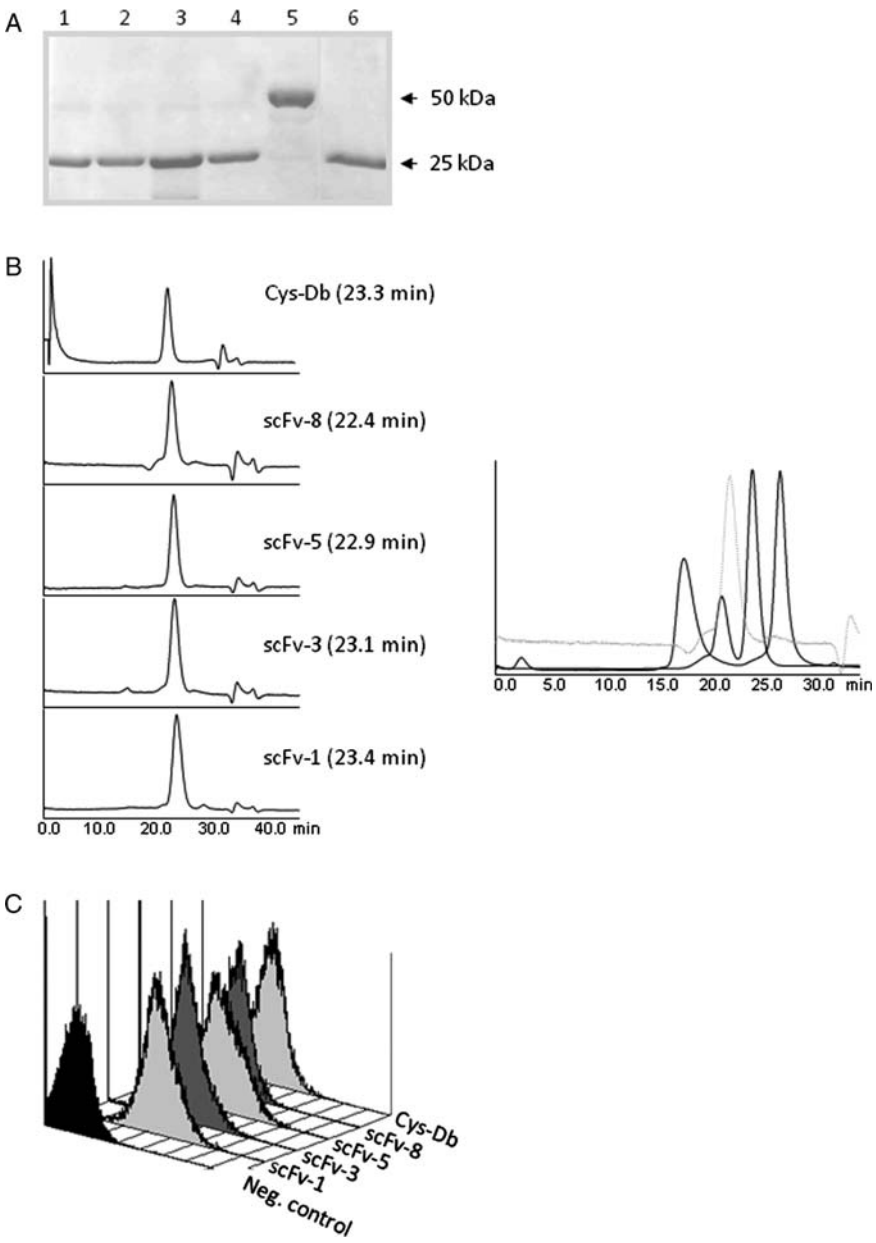

Fig. 2. Biochemical characterization of the anti-CD20 scFv variants. (**A**) SDS–PAGE gel stained with MicrowaveBlue. Lane 1, scFv-1; lane 2, scFv-3; lane 3, scFv-5; lane 4, scFv-8; lane 5, non-reduced Cys-Db; lane 6, reduced Cys-Db. (**B**) Size-exclusion chromatography on a Superdex-75 column. Elution times are shown in parentheses. The gel filtration of the molecular markers β-Amylase (200 kDa; 18.1 min), Alcohol Dehydrogenase (150 kDa; 21.8 min), Carbonic Anhydrase (29 kDa; 24.7 min) and Cytochome c (12.4 kDa; 27.4 min) with the scFv-8 trace indicated in grey are shown on the right side. (**C**) Flow cytometry of 38C13-huCD20 cells incubated with scFv variants.

Negative control was secondary antibody only. Saturation binding studies, conducted on CD20-positive cells using flow cytometry, confirmed that the scFv dimers retained effective affinities comparable to the parental antibody (data not shown).

In vivo characterization of anti-CD20 diabodies

MicroPET imaging using ^{124}I-labeled anti-CD20 Db Imaging with the anti-CD20 scFv-8 dimer was carried out at 8 h p.i. (Fig. 3A). Four mice carrying CD20-positive tumors averaging 182($\pm$120) mg in weight and CD20-negative tumors averaging 106($\pm$58) mg in weight were injected with 96–98 μCi of ^{124}I-labeled scFv-8 dimer (specific activity = 3.33 μCi/μg). Following the scan at 8 h p.i., mice were sacrificed and tumors, blood and organs were excised and the percent ID/g was calculated (Fig. 3A). The average uptake in the CD20-positive tumors was 3.9 ($\pm$1.1)% ID/g, which was significantly higher than the uptake by control CD20-negative 38C13 tumors of 2.3($\pm$0.6)% ID/g ($P = 0.024$). This resulted in a positive tumor to negative tumor uptake ratio of 1.7($\pm$0.1). However, the activity in the blood was relatively high [3.0($\pm$1.1)% ID/g] and not significantly different from the activity in the positive tumor ($P = 0.144$). Thus, the positive tumor to blood ratio was only 1.4($\pm$0.4). ROIs were drawn on the images and the positive tumor to negative tumor ratio was determined to be 1.6($\pm$0.5), while the positive tumor to soft tissue ratio was 2.5($\pm$0.7).

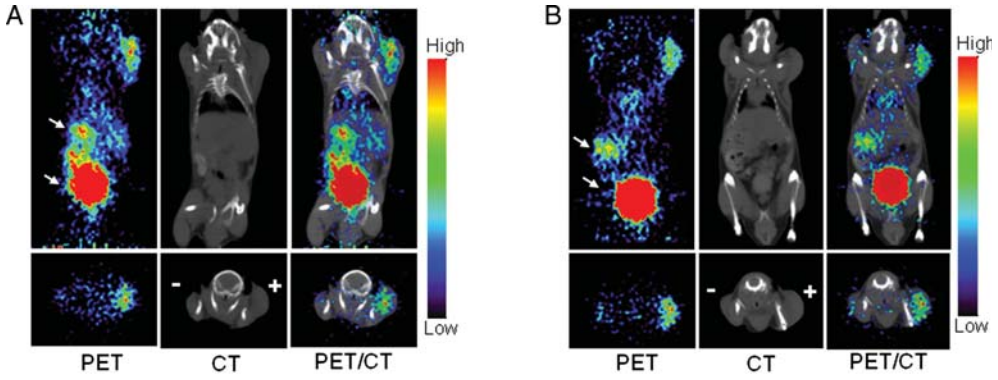

^{124}I-Diabody ($n = 4$)

Organ	Bio (8h)[a]	Ratios[b]
38C13-huCD20	3.9(1.1)	
38C13	2.3(0.6)	1.7
Blood	3.0(1.1)	1.3
Liver	1.1(0.4)	3.7
Spleen	1.3(0.5)	3.1
Kidney	4.6(1.7)	0.8
Lung	1.8(0.7)	2.1

^{124}I-Cys-Diabody ($n = 4$)

Organ	Bio (8h)[a]	Ratios[b]
38C13-huCD20	2.2(0.6)	
38C13	1.0(0.4)	2.2
Blood	1.8(0.2)	1.2
Liver	0.6(0.1)	3.7
Spleen	0.7(0.3)	3.1
Kidney	1.6(0.5)	1.3
Lung	1.3(0.2)	1.7

[a]Uptake as measured by *ex vivo* weighing and counting tissues in γ-counter
[b]Positive tumor to tissue ratios
Uptakes are expressed as % ID/g (SD)

Fig. 3. Small animal PET and CT images of mice bearing 38C13-huCD20 (right shoulder) and wild-type 38C13 (left shoulder) tumors at 8 h after administration of radioiodinated anti-CD20 Db (**A**) and Cys-Db (**B**). Coronal (upper panels) and transverse (lower panels) slices are shown. Activities in bladder and stomach are indicated by arrows. The biodistribution of the radioiodinated proteins at 8 h and the CD20-positive tumor to organ ratios are shown in the tables below. ID, injected dose; SD, standard deviation.

MicroPET imaging using ^{124}I-labeled anti-CD20 Cys-Db The Cys-Db was also evaluated by microPET imaging at 8 h after tail-vein injection (Fig. 3B). Four mice carrying CD20-positive tumors of 70($\pm$7) mg and CD20-negative tumors of 34($\pm$9) mg in weight were injected with 128–131 μCi of ^{124}I-labeled Cys-Db (specific activity = 5.4 μCi/μg) and sacrificed after the scan. The percent ID/g of radioactive uptakes in tumors, blood and normal tissues at the time of sacrifice (8 h) are shown in Fig. 3B. In these mice, the uptakes in the CD20-positive and CD20-negative tumors were 2.2($\pm$0.6) and 1.0($\pm$0.4)% ID/g, respectively, which was significantly different ($P = 0.011$) and resulted in a ratio of 2.2. The activity in the blood was 1.8($\pm$0.2)% ID/g which was not significantly different from the uptake in the positive tumor ($P = 0.170$) resulting in a ratio of 1.2. ROIs drawn on the images yielded a positive to negative tumor ratio of 1.8($\pm$0.2) and a positive tumor to soft tissue ratio of 3.2($\pm$0.7).

Biodistribution of ^{131}I-labeled anti-CD20 Cys-Db The biodistribution of the Cys-Db was evaluated at different time points and the results are shown in Fig. 4A. The overall trend is less activity in all tissues over time with the highest uptake in the CD20-positive tumor from 4 to 10 h. At 20 h, the CD20-positive to CD20-negative tumor ratio was 4.75. However, the activities in all tissues, including the tumors, were below 1% ID/g. The blood activity of the^{131}I-anti-CD20 Cys-Db at different time points was plotted against the blood activity of the ^{131}I-anti-CEA Cys-Db which has a beta-half-life of 2.68 h (Olafsen *et al.*, 2004a). Figure 4B shows that both Cys-Dbs have similar activities in the blood from 4 to 20 h p.i.

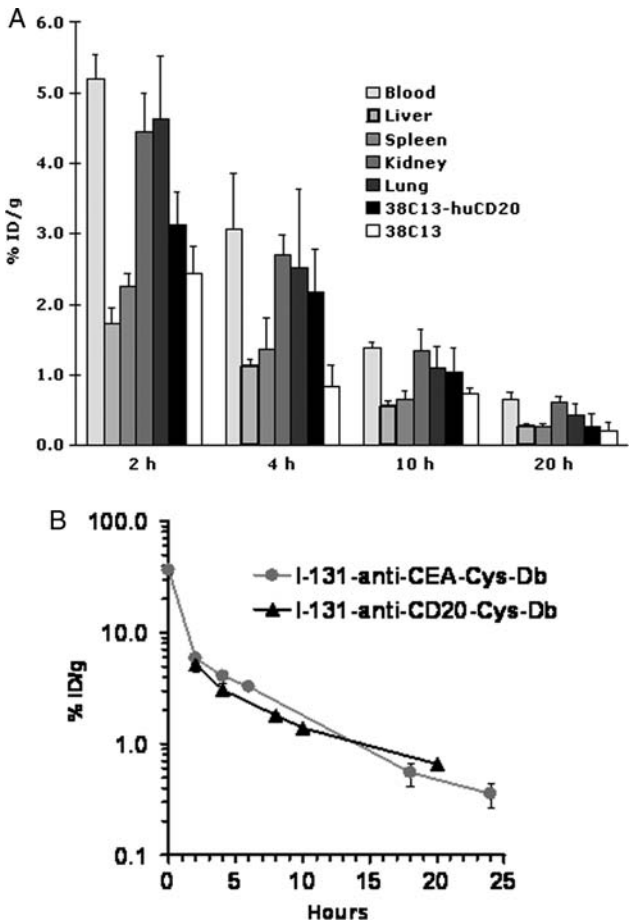

Fig. 4. Tissue biodistribution (**A**) and blood activity (**B**) of ^{131}I-labeled Cys-Db in groups of four C3Hf/Sed/Kam mice per time point. The blood activity of anti-CEA Cys-Db is shown for comparison in (**B**).

Discussion

This work describes the engineering of five anti-CD20 scFv formats; four that differed in the linker length between the variable domains and one that contained a C-terminal cysteine preceded by a short linker as previously described (Olafsen *et al*., 2004a). The scFv were all designed in the V_L-V_H orientation and the linker lengths were one, three, five and eight residues. Although linker lengths of <12 residues will generally force dimerization of the scFv fragments, we have observed that linkers of eight residues can produce a mixture of monomers and dimers and that the ratio between the two species was concentration-dependent (Leyton *et al*., 2009). For this reason, we decided to engineer another anti-CD20 scFv fragment with the more commonly used linker length of five amino acids. Size exclusion chromatography showed that both fragments eluted as one population corresponding to a scFv dimer of $\sim$50 kDa. The intent of shortening the linker to one and three residues was to generate higher orders of multimers such as triabodies and tetrabodies with a higher functional affinity than that of intermediate-sized antibody fragments, such as the minibody (80 kDa) and scFv-Fc (105 kDa) (Wu and Senter, 2005). However, size exclusion chromatography revealed that both scFv-1 and scFv-3 were also only associating into dimers. This can partially be explained by the orientation of the V genes in the scFv fragment. Indeed, the transition to dimer and higher orders of oligomers was found not to be distinct for an anti-neuraminidase NC10 scFv in V_L-V_H orientation as opposed to that of the reversed orientation (Dolezal *et al*., 2000). Both 2- and 1-residue linked NC10 scFv V_L-V_H formed a mixture of dimers, trimers and tetramers, whereas the linker-less and 3-residue versions formed almost exclusively tetramers and dimers, respectively. In other studies, a linker-less anti-CD22 scFv V_L-V_H formed an almost pure dimer population (Arndt *et al*., 2004), whereas a linker-less anti-Lewis Y sc Fv V_L-V_H formed a mixture of trimers and tetramers (Kelly *et al*., 2008). Hence, the pattern of oligomerization appears to be highly variable among different antibodies, and a linker-less anti-CD20 scFv V_L-V_H may still not have resulted in oligomerization. Analysis of solved scFv crystal structures has shown that the V_L-V_H bridging distance (i.e. V_L C-terminal to V_H N-terminal) is $5-10$ Å less than the corresponding V_H-V_L distance (Huston *et al*., 1995). Therefore, one would expect that the scFv V_L-V_H fragments would favor a greater proportion of higher orders of multimers, due to the greater constraint. Since this is clearly not the case, other factors such as the C-terminal residues and V-domain interface interaction have been suggested to affect the flexibility and stoichiometry of scFv oligomers (Dolezal *et al*., 2000).

The scFv-8 dimer and the Cys-Db were evaluated for their *in vivo* tumor targeting by microPET imaging. When both fragments were randomly radioiodinated on tyrosine residues with ^{124}I, we observed that the Cys-Db had a slightly better radiolabeling efficiency. In addition, the immunoreactivity of the Cys-Db (40%) was superior to that of the scFv-8 dimer (29%) following iodination. These favorable properties were extended into the animals, where the Cys-Db gave a better positive to negative tumor ratio (2.2) than the scFv-8 dimer (1.7) at 8 h p.i. Their tumor to blood and normal tissues ratios were otherwise similar. Thus, it appears that the C-terminal disulphide bond does not impair the *in vivo* performance of the anti-CD20 diabody. Moreover, Cys-Dbs against additional targets (i.e. CEA and Her2/neu) have demonstrated that they retain their function both *in vitro* and *in vivo* (Olafsen *et al*., 2004a,b; Sirk *et al*., 2008). Thus, the bifunctionality (i.e. antigen specificity and site-specific modification) offered by this format appears to be a general feature that can be applied to any diabody.

We have recently described the engineering of two intermediate-sized anti-CD20 antibody fragments (minibody and scFv-Fc) that were evaluated by microPET in the same animal model (Olafsen *et al*., 2009). Due to their longer half-lives, excellent high-contrast images were obtained the next day at 21 h. However, the objective of this work was to generate and evaluate immunoPET tracers that could be used for same-day imaging. Here, we obtained high contrast images at 8 h after administration. At 20 h, the radioactive uptake of ^{131}I-Cys-Db in the positive tumor was less than 1% ID/g as verified by the biodistribution. Similar tumor uptake activities were also observed with ^{124}I-labeled anti-prostate stem cell antigen diabodies at 20 h (Leyton *et al*., 2009). This observation is not absolute though, as higher tumor activities [4.5(0.5)% ID/g] have been obtained with ^{124}I-labeled anti-CEA Db at 18 h p.i. (Sundaresan *et al*., 2003). Factors that can affect tumor retention are antigen expression, internalization and dehalogenation of the radiolabeled tracer. Since CEA and CD20 are considered to be non-internalizing, the difference in tumor uptake is probably due to antigen expression. Indeed, the CEA-positive human LS174T colon cancer cells express 5×10^5 CEA molecules on the surface (Berk *et al*., 1997), whereas we observed that the 38C13-huCD20 cells express about 50% less than that of Daudi (6×10^4 CD20/Daudi cell) (Bubien *et al*., 1993) based on mean fluorescence intensity (unpublished data).

Overall, the CD20 antigen is an attractive target candidate for immunoimaging and/or immunotherapy of B-cell lymphomas as it does not shed or internalize upon antibody binding. The anti-CD20 diabodies generated here extend the repertoire of reagents for non-invasive imaging of lymphomas that can potentially improve detection, especially of low-grade lymphomas. The advantage of the Cys-Db is that site-specific modification will provide a tracer with high immunoreactivity. In addition, diabodies radiolabeled with ^{18}F would produce an immunoPET tracer with compatible biological and physical half-lives. This work shows that specific tumor targeting was achieved, suggesting potential clinical utility of these molecules for same-day imaging of CD20-positive lymphomas.

Acknowledgements

The authors would like to thank Felix B. Salazar for excellent technical support. We are especially grateful to Dr David Stout and Judy Edwards at the Crump Institute for Molecular Imaging at UCLA for the use and assistance with the microPET/CT. Thanks are also extended to the UCLA Jonsson Comprehensive Cancer Center and Center for AIDS Research Flow Cytometry Core Facility at UCLA.

Funding

This work was supported by NIH Grants P50 CA107399, P50 CA086306, CA119367, and the Margaret Early Medical

Research Trust. A.A.R. is a member of the City of Hope Comprehensive Cancer Center (CA 33572). J.M.T. and A.M.W. are members of Jonsson Comprehensive Cancer Center (CA 16042). J.M.T. is a Damon Runyon Clinical Investigator supported in part by the Damon Runyon Cancer Research Foundation (CI-26-05).

References

Adams,G.P., McCartney,J.E., Tai,M.S., Oppermann,H., Huston,J.S., Stafford,W.F., 3rd, Bookman,M.A., Fand,I., Houston,L.L. and Weiner,L.M. (1993) *Cancer Res.*, **53**, 4026–4034.

Adams,G.P., Schier,R., McCall,A.M., Crawford,R.S., Wolf,E.J., Weiner,L.M. and Marks,J.D. (1998) *Br. J. Cancer*, **77**, 1405–1412.

Arndt,K.M., Muller,K.M. and Pluckthun,A. (1998) *Biochemistry*, **37**, 12918–12926.

Arndt,M.A., Krauss,J. and Rybak,S.M. (2004) *FEBS Lett.*, **578**, 257–261.

Bergman,Y. and Haimovich,J. (1977) *Eur. J. Immunol.*, **7**, 413–417.

Berk,D.A., Yuan,F., Leunig,M. and Jain,R.K. (1997) *Proc. Natl Acad. Sci. USA*, **94**, 1785–1790.

Bird,R.E., Hardman,K.D., Jacobson,J.W., Johnson,S., Kaufman,B.M., Lee,S.M., Lee,T., Pope,S.H., Riordan,G.S. and Whitlow,M. (1988) *Science*, **242**, 423–426.

Bubien,J.K., Zhou,L.J., Bell,P.D., Frizzell,R.A. and Tedder,T.F. (1993) *J. Cell Biol.*, **121**, 1121–1132.

Dolezal,O., Pearce,L.A., Lawrence,L.J., McCoy,A.J., Hudson,P.J. and Kortt,A.A. (2000) *Protein Eng.*, **13**, 565–574.

Holliger,P., Prospero,T. and Winter,G. (1993) *Proc. Natl Acad. Sci. USA*, **90**, 6444–6448.

Huston,J.S., *et al*. (1988) *Proc. Natl Acad. Sci. USA*, **85**, 5879–5883.

Huston,J.S., George,A.J.T., Tai,M-S., McCartney,J.E., Jin,D., Segal,D.M., Keck,P. and Oppermann,H. (1995) Single-chain Fv design and production by preparative folding. In Borrebaeck,C.A.K. (ed.), *Antibody Engineering*. Oxford University Press, Inc, New York, pp. 186–191.

Kelly,M.P., Lee,F.T., Tahtis,K., Power,B.E., Smyth,F.E., Brechbiel,M.W., Hudson,P.J. and Scott,A.M. (2008) *Cancer Biother. Radiopharm.*, **23**, 411–423.

Kenanova,V., *et al*. (2005) *Cancer Res.*, **65**, 622–631.

Kortt,A.A., Malby,R.L., Caldwell,J.B., Gruen,L.C., Ivancic,N., Lawrence,M.C., Howlett,G.J., Webster,R.G., Hudson,P.J. and Colman,P.M. (1994) *Eur. J. Biochem.*, **221**, 151–157.

Leyton,J.V., Olafsen,T., Sherman,M.A., Bauer,K.B., Aghajanian,P., Reiter,R.E. and Wu,A.M. (2009) *Protein Eng. Des. Sel.*, **22**, 209–216.

Li,L., Olafsen,T., Anderson,A.L., Wu,A., Raubitschek,A.A. and Shively,J.E. (2002) *Bioconjug. Chem.*, **13**, 985–995.

Loening,A.M. and Gambhir,S.S. (2003) *Mol. Imaging*, **2**, 131–137.

Olafsen,T., *et al*. (2004a) *Protein Eng. Des. Sel.*, **17**, 21–27.

Olafsen,T., Tan,G.J., Cheung,C.W., Yazaki,P.J., Park,J.M., Shively,J.E., Williams,L.E., Raubitschek,A.A., Press,M.F. and Wu,A.M. (2004b) *Protein Eng. Des. Sel.*, **17**, 315–323.

Olafsen,T., Kenanova,V.E. and Wu,A.M. (2006) *Nat. Protoc.*, **1**, 2048–2060.

Olafsen,T., Betting,D., Kenanova,V.E., Salazar,F.B., Clarke,P., Said,J., Raubitschek,A.A., Timmerman,J.M. and Wu,A.M. (2009) *J. Nucl. Med.*, **50**, 1500–1508.

Robinson,M.K., Doss,M., Shaller,C., Narayanan,D., Marks,J.D., Adler,L.P., Gonzalez Trotter,D.E. and Adams,G.P. (2005) *Cancer Res.*, **65**, 1471–1478.

Sirk,S.J., Olafsen,T., Barat,B., Bauer,K.B. and Wu,A.M. (2008) *Bioconjug. Chem.*, **19**, 2527–2534.

Sundaresan,G., Yazaki,P.J., Shively,J.E., Finn,R.D., Larson,S.M., Raubitschek,A.A., Williams,L.E., Chatziioannou,A.F., Gambhir,S.S. and Wu,A.M. (2003) *J. Nucl. Med.*, **44**, 1962–1969.

Whitlow,M., Filpula,D., Rollence,M.L., Feng,S.L. and Wood,J.F. (1994) *Protein Eng.*, **7**, 1017–1026.

Worn,A. and Pluckthun,A. (1999) *Biochemistry*, **38**, 8739–8750.

Wu,A.M. and Senter,P.D. (2005) *Nat. Biotechnol.*, **23**, 1137–1146.

Wu,A.M., Chen,W., Raubitschek,A., Williams,L.E., Neumaier,M., Fischer,R., Hu,S.Z., Odom-Maryon,T., Wong,J.Y. and Shively,J.E. (1996) *Immunotechnology*, **2**, 21–36.

Yazaki,P.J., Wu,A.M., Tsai,S.W., Williams,L.E., Ikler,D.N., Wong,J.Y., Shively,J.E. and Raubitschek,A.A. (2001) *Bioconjug. Chem.*, **12**, 220–228.